Study of the conductance and structure characteristics of C_{60}/Sb bilayers

2001 J. Phys.: Condens. Matter 13 3987

(http://iopscience.iop.org/0953-8984/13/18/309)

INSTITUTE OF PHYSICS PUBLISHING JOURNAL OF PHYSICS: CONDENSED MATTER

J. Phys.: Condens. Matter **13** (2001) 3987–4000 www.iop.org/Journals/cm PII: S0953-8984(01)18352-9

Study of the conductance and structure characteristics of C_{60}/Sb bilayers

Xiang Li[1,2,4], H Wang[1], W N Wang[1], Y J Tang[1], H W Zhao[1], W S Zhan[1] and J G Hou[2]

[1] State Key Laboratory for Magnetism, Institute of Physics and Centre for Condensed Matter Physics, Chinese Academy of Science, Beijing, 100080, People's Republic of China
[2] Structure Research Laboratory, University of Science and Technology of China, Hefei, Anhui, 230026, People's Republic of China

E-mail: xli@g203.iphy.ac.cn (Xiang Li)

Received 29 November 2000, in final form 14 March 2001

Abstract

The electrical and structural properties of C_{60}/Sb bilayers were investigated. *In situ* direct-current conductivity measurement results indicate that the doping of Sb into C_{60} induces the C_{60} order–disorder phase transition temperature to increase to ∼278 K. According to the results of a transmission electron microscope and atomic force microscope study, such a transition (near 278 K) implies the formation of an interfacial structure of Sb-doped C_{60}. Annealing and the absorption of gases destroy the interfacial structure of Sb-doped C_{60}. A possible mechanism for such a phase transition is discussed.

1. Introduction

The unique structure and characteristics of C_{60} and C_{60} derivatives have attracted much scientific attention [1–6]. Below and above 260 K, C_{60} can be fabricated in the simple cubic (sc) and face-centred-cubic (fcc) structural forms, respectively. C_{60} crystal undergoes an orientational order–disorder (fcc–sc) phase transition between the sc and fcc forms at 260 K, as demonstrated by many experiments [1, 7–9]. Differential scanning calorimetry (DSC) results showed that the width of the fcc–sc transition for C_{60} crystal is ∼0.4 K [8], while dc conductance measurement results indicated a transition width of ∼2–3 K [10]. The reasons for the different widths were explored by previous research [10]; the authors of [10] asserted that the electrical properties are more sensitive to structure change than the heat capacity. However, Mort *et al* studied the dc conductivity of C_{60}/C_{70} films and found that the fcc–sc transition occurred in the range 270 K–300 K [11], and they asserted that the large width is a consequence of significant lattice distortion of the C_{60} crystal. It is reported that some fullerides exhibit a phase transition similar to that of pristine C_{60}. For example, structure transitions occur near 299 K and 305 K

[4] Author to whom any correspondence should be addressed, at: State Key Laboratory for Magnetism, Institute of Physics and Centre for Condensed Matter Physics, Chinese Academy of Science, Beijing, 100080, PO Box 603, People's Republic of China. Telephone: 86-010-82649251; fax: 86-010-82649485.

0953-8984/01/183987+14$30.00

in Na_2CsC_{60} and Na_2KC_{60}, respectively [4]. Doping with O_2 leads to the formation of $C_{60}O$, which undergoes a C_{60}-like phase transition at 270 K [12, 13]. Furthermore, research on Ar-doped C_{60} single crystal indicated that doping with Ar causes a drop of the C_{60} fcc–sc transition temperature [14].

In this paper, results from an investigation of the C_{60}–Sb interaction are presented. Sb is reported to be an effective surfactant in the growth of high-quality and larger-scale C_{60} single-crystal films at the surfaces of NaCl single crystal and mica. In the literature it is reported that the C_{60}–Sb interaction is complex. The effect of such an interaction on the electrical properties of Sb-doped C_{60} crystal films is of interest and is a question that remains open. The effect of Sb incorporation in C_{60} is crucial for the application of such C_{60} films and is well worth studying. The paper is organized as follows. Section 2 describes the experiments, section 3 gives the results, section 4 is a discussion, and section 5 gives our conclusions.

2. Experiments

The films were prepared by the two-source thermal co-evaporation method under a vacuum of 3.0×10^{-6} Torr. The purities of the Sb and C_{60} were 99.999% and 99.9% respectively. The substrate was freshly cleaved mica and was kept at 450 K during evaporation. Four pre-deposited gold pads were deposited upon the mica substrate as electrodes for conductance measurement. A quartz oscillation monitor was used to calibrate the deposition rates and thicknesses of the films. The resolution of the monitor is 0.1 nm. First a layer of Sb was deposited with the thickness of 3–10 nm, and a few minutes later a layer of C_{60} film was deposited at a rate of 1 nm min^{-1}. The thickness of the C_{60} film was in the range 10–20 nm. The resulting sample was kept at 450 K for 30 minutes before being cooled down to 130 K. The dc conductance measurement was performed using a standard four-wire configuration with computer-controlled Keithley 2400 and Keithley 6517A meters. The morphology of the films was analysed under ambient conditions using an atomic force microscope (AFM), Autopobe CP (Park Instruments), in contact mode, with a scanning frequency of 1.2 Hz. A Hitachi H-800 TEM was used for structure characterization.

3. Results

3.1. Conductance investigation

Figure 1 shows the logarithm of the electrical conductance ($\ln \sigma$) versus the reciprocal temperature ($1/T$) for C_{60}(10 nm)/Sb(3 nm). Figure 1(a) shows the results from the first measurement process. After the first measurement process, the sample was annealed at 450 K for five hours; then the second measurement cycle was performed and the results are shown in figure 1(b). The results in figures 1(a) and 1(b) were all measured *in situ*. When the second measurement cycle was finished, the sample was exposed to air, then degassed in a vacuum, and then measurements were made; the results are presented in figure 1(c). In figure 1(a), the fcc–sc phase transition of C_{60} is observed clearly near 260 K—it leads to a conductance anomaly—and the temperature width of this transition is $\sim$15 K, much larger than that for single-crystalline C_{60}. The large width of the transition presumably results from the poor quality of the C_{60} film. From figure 1(a), the activation energies are, below and above 263 K, 0.172 eV and 0.379 eV, respectively—considerably smaller than those of pristine C_{60} [10]. The small activation energies of the film also indicate that some Sb may be incorporated in the C_{60} crystal. The most interesting feature of figure 1(a) is the observation of the jump near 278 K. Comparing figure 1(a) with figure 1(b), we see that annealing increases the conductance

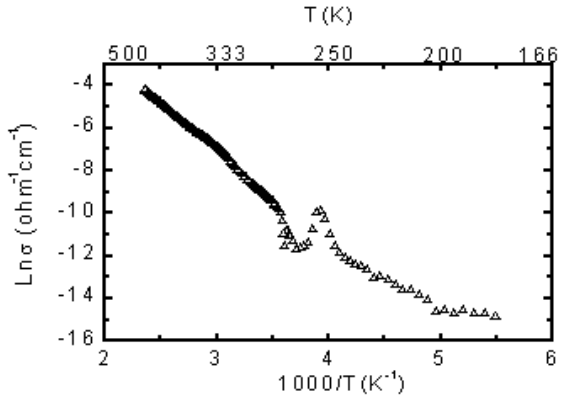

(a)

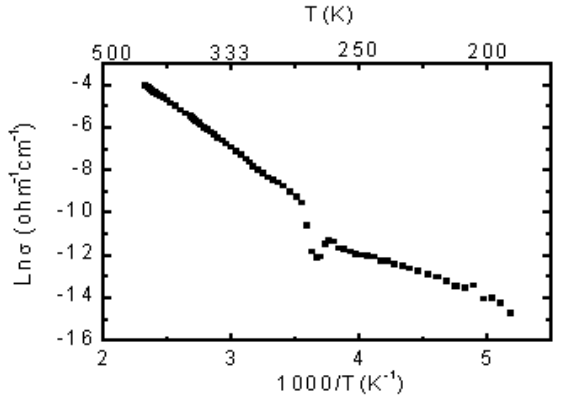

(b)

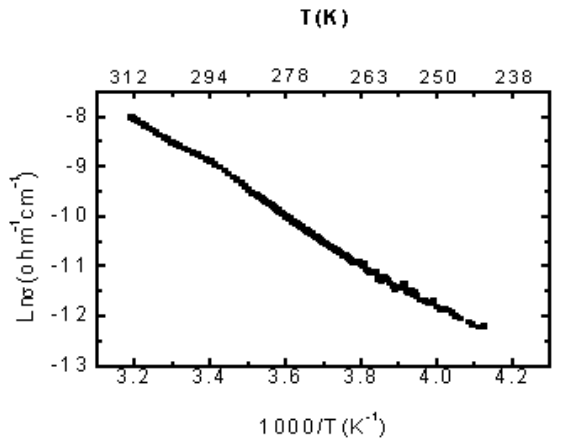

(c)

Figure 1. $\ln\sigma$–$1/T$ results for C_{60}(10 nm)/Sb(3 nm) bilayers. (a) The first *in situ* measurement cycle. The conductance anomaly jumps are in the ranges 255–269 K and 275–277 K. (b) The sample annealed at 450 K before the measurements were made *in situ*; the anomalous conductance jump is in the range 266–273 K. (c) The sample exposed to air and degassed in vacuum before the measurements were made. The anomalous jump of the conductance near 260 K is blurred. $T_s = 450$ K.

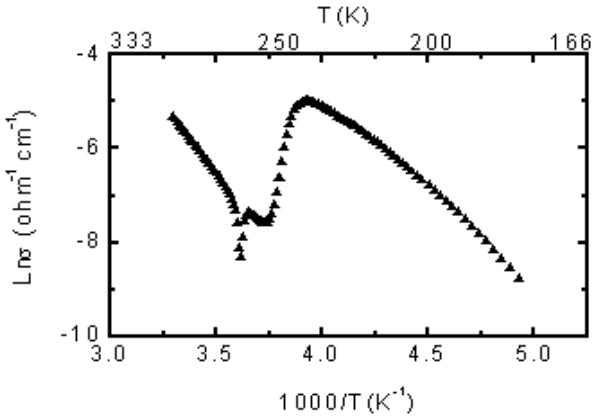

(a)

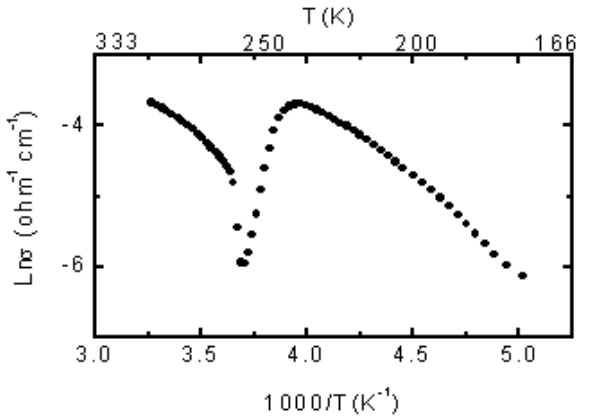

(b)

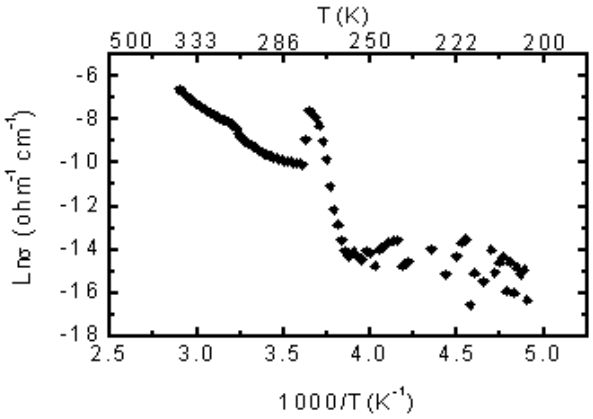

(c)

Figure 2. $\ln\sigma$–$1/T$ for C_{60}(20 nm)/Sb(10 nm) bilayers. (a) The first *in situ* measurement cycle. The conductance anomaly jumps are in the ranges 255–268 K and 273–277 K. (b) The sample annealed at 450 K before the measurements were made *in situ*; the anomalous conductance jump is in the range 255–270 K and much enhanced. (c) The results for the sample exposed to air and degassed in vacuum before the measurements were made. $T_s = 450$ K.

slightly and reduces the conductance jump near 278 K. Moreover, the transition in the range 266 K–272 K is very much compressed and widened, and the activation energies are increased a little. From figure 1(c), we see that the conductance jump near 260 K is suppressed and its value decreases by about four orders of magnitude, while the activation energy is 0.420 eV, much larger than those for figures 1(a) and 1(b). These results indicate that the adsorption of air significantly affects the phase transition of C_{60}.

Figure 2 shows $\ln\sigma$–$1/T$ results for C_{60}(20 nm)/Sb(10 nm). Figure 2(a) shows the results from the first measurement cycle. Figure 2(b) shows the results for the sample annealed at 450 K for five hours before the measurements. Figure 2(c) shows the results for the sample exposed to air then degassed in vacuum before the measurements. From figure 2(a), it is obvious that the two conductance jumps appeared and were enhanced compared with those in figure 1(a). Compare figure 2(a) with figure 2(b): annealing causes the jump near 260 K to be enhanced and sharpened while the jump near 275 K disappears, and annealing also increases the conductance of the film a little. Figure 2(c) indicates that the conductance dropped by about five orders when the films were exposed to air. Below and above 300 K, the activation energies are several meV and about 1 eV, respectively.

Figure 3 shows $\ln\sigma$–$1/T$ for C_{60}(20 nm)/Sb(15 nm). Figure 3(a) shows the results from the first measurement process, and figure 3(b) shows the results for the sample annealed *in situ* for nine hours before the measurements. Figure 3(c) shows the results for the sample exposed to air then degassed in vacuum before the measurements. In figure 3(a), two conductance jumps appear in the ranges 258 K–262 K and 262 K–274 K. Following annealing, the jumps observed in figure 3(b) can no longer be clearly distinguished and are moved to the range 263 K–273 K. In figure 3(c), the activation energies below and above 300 K are $\sim$45 meV and $\sim$1.06 eV, respectively.

Figure 4 shows $\ln\sigma$–$1/T$ for C_{60}(60 nm)/Sb(1.5 nm). Figures 4(a)–4(c) show results from measurement processes similar to those of figure 3. In figure 4(a), two conductance jumps are observed in the ranges 263 K–269 K and 280 K–283 K. The linearity of $\ln\sigma$–$1/T$ is very poor compared with that in figure 1. In figure 4(b), only one jump is observed, in the range 256 K–279 K. In figure 4(c), the activation energies below and above 300 K are $\sim$45 meV and 1.1 eV, respectively. After the sample was heated to 450 K and then the temperature dropped, the slope of the graph was smaller than that for the increasing-temperature process. The temperature-drop process in figure 4(c) indicates that the absorbed air can be partly caused to desorb by annealing. The desorption of air from the film increases its conductance and decreases its activation energy.

3.2. Microstructure and surface morphology

Figure 5 shows AFM images of C_{60}/Sb. Figures 5(a), 5(b), 5(c) are images of C_{60}(20 nm)/Sb(1.0 nm), C_{60}(20 nm)/Sb(3.5 nm), C_{60}(20 nm)/Sb(5.0 nm), respectively. The images indicate that C_{60} film grown upon 1.0 nm Sb has a size of 270 ± 30 nm; C_{60} film grown upon 3.5 nm Sb has a size of 470 ± 30 nm—larger than that in figure 5(a); and in the case of C_{60} film grown upon 5.0 nm Sb the size is 133 ± 30 nm—much smaller than that of figures 5(a) and 5(b). AFM images reveal that in figure 5(a) the morphology of the film has the typical characteristics of an island growth mode, while in figure 5(b) the surface of the film is more planar and smooth compared with that in figure 5(a), showing pronounced characteristics of a layer-by-layer growth mode. Furthermore, in figure 5(c) the grain size of C_{60} in the film is much smaller than those in figures 5(a) and 5(b), and its microstructure has the characteristic of high uniformity. Xu *et al* have discussed the different growth behaviours of C_{60} on the different Sb films in detail [15, 17, 18]. Our results are consistent with the previous reports. Comparing figures 5(a)–5(c),

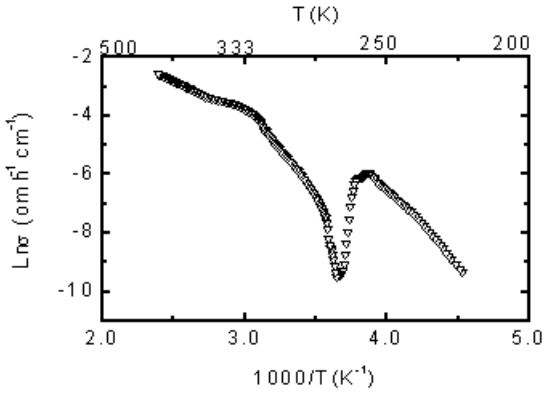

(a)

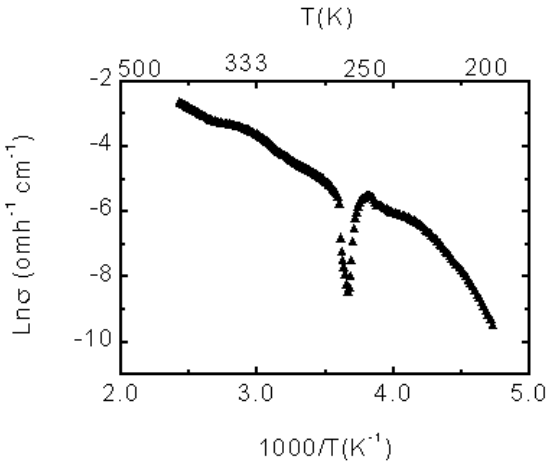

(b)

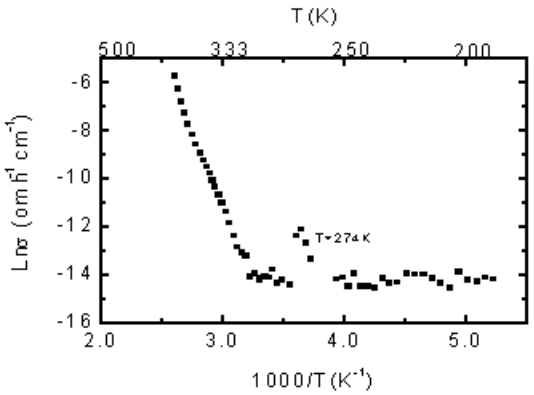

(c)

Figure 3. $\ln\sigma$–$1/T$ results for C_{60}(20 nm)/Sb(15 nm) bilayers. (a) The first *in situ* measurement cycle. The conductance anomaly jumps are in the ranges 258–262 K and 262–274 K. (b) The sample annealed at 450 K before the measurements were made *in situ*; the anomalous conductance jump is in the range 263–273 K. (c) The results for the sample exposed to air and degassed in vacuum before the measurements were made. $T_s = 450$ K.

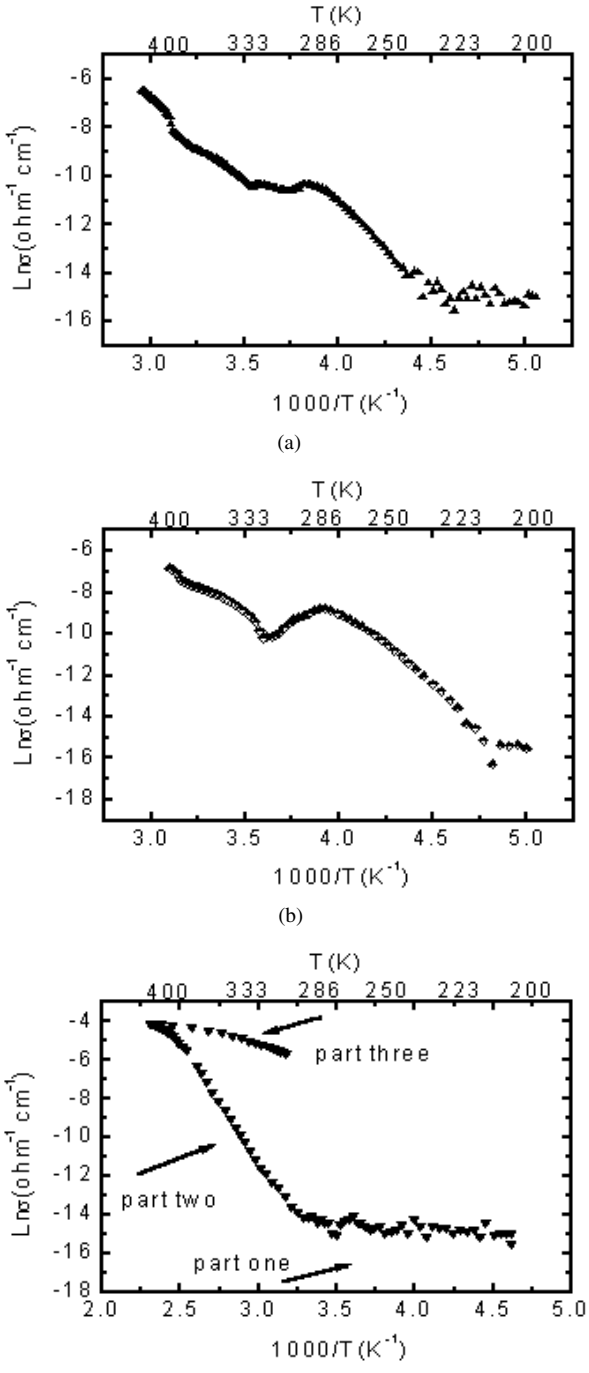

Figure 4. $\ln\sigma$–$1/T$ results for C_{60}(60 nm)/Sb(1.5 nm) bilayers. (a) The first *in situ* measurement cycle. The conductance anomaly jumps are in the ranges 263–268 K and 280–283 K. (b) The sample annealed at 450 K before the measurements were made *in situ*; the anomalous conductance jump is in the range 256–270 K. (c) The results for the sample exposed to air and degassed in vacuum before the measurements were made. $T_s = 450$ K.

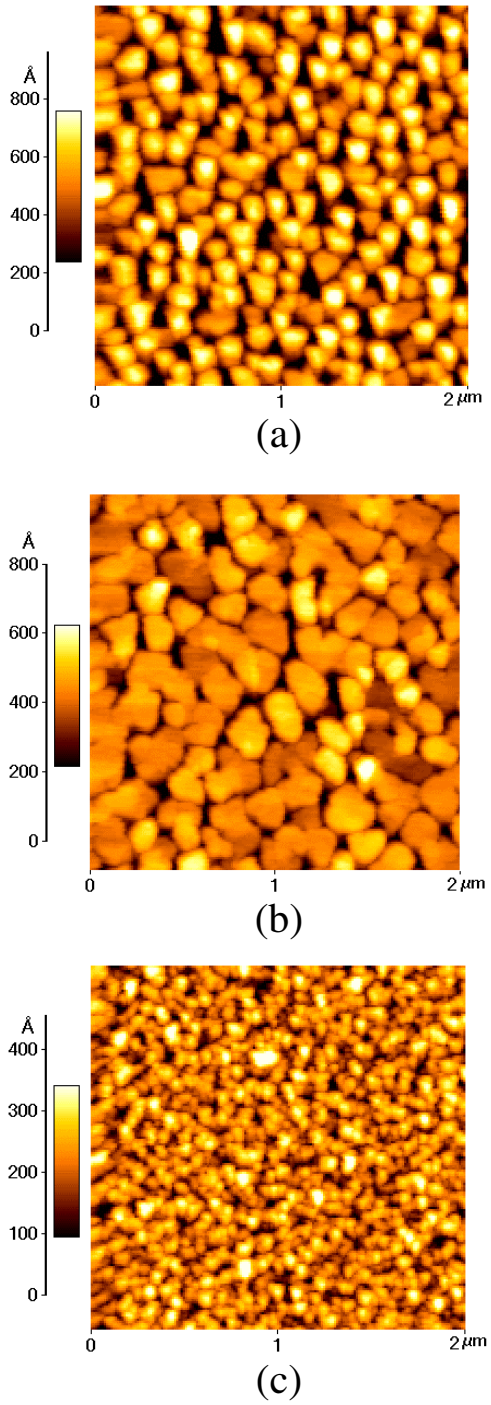

Figure 5. AFM images of C_{60}/Sb deposited at the substrate temperature of 450 K. (a), (b), (c) Images of C_{60}(20 nm)/Sb(1.0 nm), C_{60}(20 nm)/Sb(3.5 nm), C_{60}(20 nm)/Sb(5.0 nm), respectively; $T_s = 450$ K. With increasing thickness of the Sb layer, the C_{60} film changed from rough to planar and smooth, then to rough again; the grain size becomes smaller and smaller.

(This figure is in colour only in the electronic version, see `www.iop.org`)

we see that the presence of a moderate amount of Sb mediator significantly reduces the contact barrier of C_{60} and mica, and improves the transport of adsorbed C_{60} clusters on the surface of the substrate. On the other hand, a thick (more than 5 nm) Sb mediator increases the density of the aggregation nuclei and also induces an additional barrier to the diffusion of deposited C_{60}, which in the end reduces the average scale of the C_{60} films.

Figure 6 shows the TEM images of samples with different Sb layers. Figures 6(a)–6(c) are images of C_{60}(60 nm)/Sb(1.5 nm), C_{60}(20 nm)/Sb(3 nm), and C_{60}(20 nm)/Sb(10 nm), respectively. The SED pattern indicates that no Sb diffraction pattern can be clearly observed,

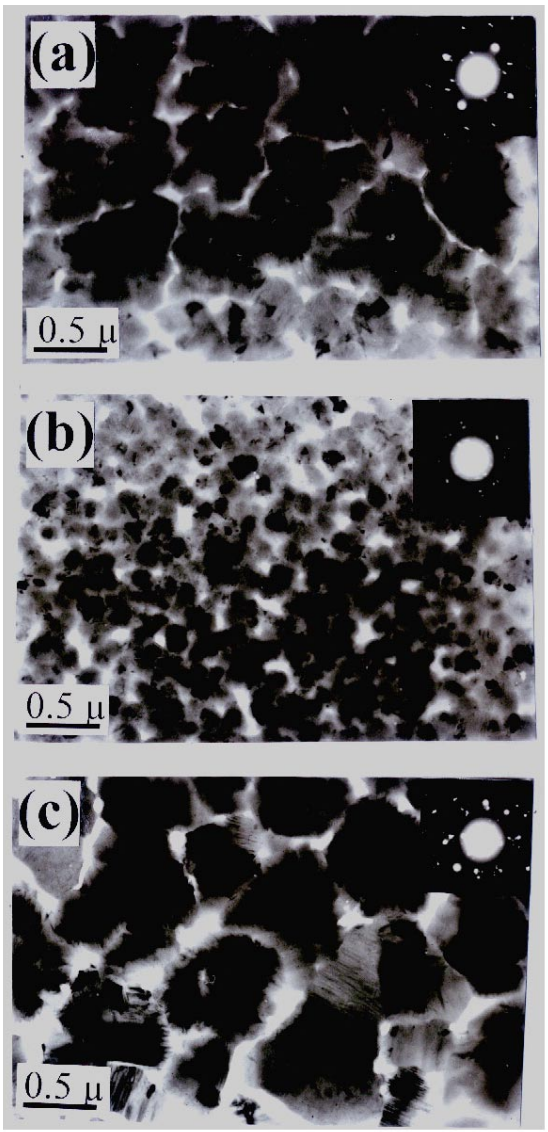

Figure 6. TEM images of (a) C_{60}(60 nm)/Sb(1.5 nm), (b) C_{60}(10 nm)/Sb(3 nm), (c) C_{60}(20 nm)/Sb(10 nm); $T_s = 450$ K. With increasing thickness of the Sb layer, the growth mode of the C_{60} changed from island to layer-by-layer then to island growth again.

which implies that Sb is uniformly dispersed in the matrix of C_{60}. The TEM images indicate that, with increase of the thickness of the Sb layer, the grain size of the film changes: first there are large islands; these give way to very smooth and planar layers, then to grains of very small sizes for the thickest Sb layer. In figure 6(a), the crystal size of C_{60} is $\sim$1.5 μm and the SED pattern demonstrated that the lattice structure of C_{60} has some distortion. In figure 6(b) the grain size of the crystalline C_{60} is about 1.3 μm; the SED pattern indicates that the C_{60} crystalline lattice is perfect. In figure 6(c), the grain size of the C_{60} crystal is $\sim$0.15 μm, and the density of the interface is very much higher than those for figures 6(a) and 6(b); the SED pattern shows that the C_{60} is polycrystalline. These results are in agreement with those from the AFM study. The structural differences between the samples before and after the annealing were also characterized by means of TEM and SED. The results showed that the annealing enhances the growth of C_{60} grains, but no significant change of the SED pattern was observed.

4. Discussion

4.1. The effect of Sb doping

Comparing figures 1–4, we see that the increase in the thickness of Sb causes the electrical conductivity of the bilayer to increase, and the magnitude of the jump near 278 K is significantly enhanced. Moreover, increasing Sb thickness increases the linear deviation of $\ln\sigma$–$1/T$ for the film and decreases its activation. The parameters of the conductance jumps, derived from figures 1–4, are listed in table 1.

Table 1. The parameters of the conductance jumps during the transition for different samples.

	Pristine-C_{60}-related transition		Novel transition	
Sample	T_1–T_2	$(\sigma_1-\sigma_2)/\sigma_2$	T_3–T_4	$(\sigma_3-\sigma_4)/\sigma_4$
C_{60}(60 nm)/Sb(1.5 nm)	263 K–268 K	34%	280 K–283 K	10.5%
C_{60}(10 nm)/Sb(3 nm)	255 K–269 K	516%	275 K–277 K	104%
C_{60}(20 nm)/Sb(10 nm)	255 K–268 K	1250%	273 K–277 K	162%
C_{60}(20 nm)/Sb(15 nm)	258 K–263 K	20%	263 K–273 K	2814%

The parameters in table 1 are as follows: T_1, T_2, T_3, and T_4 are the temperatures at which the sample conductance reaches its maxima and minima; σ_1, σ_2, σ_3, and σ_4 are the conductances corresponding to T_1, T_2, T_3, and T_4 respectively.

From the different behaviours of the anomalous conductance jumps in figures 1(a)–4(a) and the parameters presented in table 1, one can see that a thin Sb layer corresponds to a sharp conductance jump while thick-Sb-layer films correspond to large temperature widths of the transition. Meanwhile, in the thin-Sb-layer samples the dominant jump is of $\sim$260 K and in thick-Sb-layer samples the dominant jump is of $\sim$270 K. Considering the small grain size and the high density of the interface for C_{60} films, it is reasonable to assume that the jump in the higher-temperature range (263 K–273 K) is related to the doping of Sb into crystalline C_{60}.

Early work reports that noble metal aggregates at the surface of C_{60} [18]. We believe that a similar process happens which induces the disappearance of Sb from Sb/C_{60}. When noble gas is doped into C_{60} crystal, the temperature of the C_{60} fcc–sc transition drops [14]. When noble metal and O_2 are doped into C_{60} crystal, C_{60}-derived compounds form that have C_{60}-like order–disorder phase transitions, and the resulting compounds have phase transition temperatures higher than those of pristine C_{60} [3, 4, 12, 13]. Sb is used as a surfactant for

the growth of high-quantity and large-scale C_{60} single-crystal film [15, 16]. Some researchers believe that Sb efficiently enhances the interlayer diffusion in C_{60} [15–18], which favours the exchange of C_{60} and Sb in different layers. In Sb/C_{60}, some Sb remains doped into the C_{60} grains; the density of the Sb remaining is reciprocally proportional to the distance from the boundaries of the C_{60} grains. The Sb atoms remaining in the C_{60} act as defects or intercalate, distorting the C_{60} crystal lattice. Due to the small diameter of the Sb atom, the Sb doped into C_{60} crystal most probably locates at the tetrahedral or octahedral sites, just like Na, K, Cs in Na_2CsC_{60} and Na_2KC_{60} [4]. The presence of Sb intercalates in crystalline C_{60} may also induce a 'negative expansion' of its lattice, and result in a smaller C_{60}–C_{60} separation compared with that in the pristine C_{60} crystal. The C_{60} phase transition partially results from the lattice parameter changing with temperature (the lattice of fcc C_{60} is a little larger than that of sc C_{60}). The lattice expansion is one of the main reasons for the fcc–sc phase transition occurring in C_{60} [19]. Accordingly, in Sb-intercalated C_{60} crystal a higher temperature is needed to produce sufficient lattice expansion to induce a C_{60}-like phase transition, just as in the case of a high-pressure-compressed C_{60} crystal [19, 20]. There is also very probably a weak charge interaction between Sb and C_{60}. Such an interaction will hinder the rotation of C_{60} just as in the alkali–C_{60} fullerides [4] and $C_{60}O$ [12, 13], which might also be a reason for the increase of the phase transition temperature for the Sb-doped crystalline C_{60}. Consequently, the jump near 278 K in Sb/C_{60} results from incorporation of Sb in crystalline C_{60}.

Considering the results presented above, we see that the smaller the scale of the C_{60} grains, the more enhanced the jump at ∼278 K. Such results give explicit evidence that Sb is incorporated in the C_{60} crystalline lattice. In thick-Sb-layer samples, the interfacial structure of Sb-doped C_{60} dominates the properties due to the small grain size.

4.2. The effect of annealing

Compare the results in figures 1(a)–4(a) with those in figures 1(b)–4(b); annealing results in the suppression and disappearance of the jump in the high-temperature ranges (figure 1(a): 275–283 K; figure 2(a): 273–277 K; figure 3(a): 263–273 K; figure 4(a): 280–283 K). Annealing also sharpens the jump near 260 K (except in figure 1(b)). This may be because the annealing promotes the diffusion of Sb and C_{60}, and results in the separation of Sb and C_{60}, finally increasing the size of the C_{60} crystal, and improving the structure of the crystalline C_{60}.

The annealing effects for different Sb films are different. For thin-Sb-layer samples, in figure 1 the jump in the range 255 K–277 K changed to a jump in the range 266 K–272 K, indicating that annealing compresses and widens the conductance jump (in the range 255–269 K in figure 1(a)). In figure 4, in the first measurement cycle, the two conductance jumps are in the ranges 263 K–260 K and 280 K–282 K, showing that the temperature width of the jump is narrower than those in figures 2 and 3, and demonstrating that the lattices of both pristine C_{60} and Sb-doped C_{60} are perfect. Annealing blurs the difference between the two jumps in figure 4(a) and results in the jump being in the range 256 K–278 K. These results imply that annealing destroys the structure of Sb-doped C_{60} formed in the preparation of the sample and increases its conductance significantly.

For a thick-Sb-layer sample, the interface effects dominate its characteristics. For small C_{60} grains, the crystal lattice is distorted and unstable. In the Sb-doped C_{60} crystal, the high stress and plentiful defects as well as the high aggregation energy of Sb reduce the stability of the interface structure.

Annealing supplies enough energy for the diffusion of Sb and C_{60} and improves the structure of C_{60} crystallites. The high cohesion energy of Sb also favours separation of C_{60} and Sb, which results in aggregation of Sb. The exchange of Sb and C_{60} in C_{60}/Sb considerably

improves the quality of the C_{60} crystal and reduces the thickness of the layer of Sb-doped C_{60}. Such exchange finally reduces the temperature width of the C_{60} fcc–sc phase transition and results in the jump near 278 K disappearing. The annealing also reduces the density of defects and boundaries in C_{60}; thus the scattering of the charge carriers by defects and boundaries considerably decreases. Consequently, the conductance of the film significantly increases.

In addition, there is a significant difference between figure 1(b) and figures 2(b)–4(b): the annealing compresses and widens the conductance jump in the range 255–272 K (figure 1(b)). The reason for such difference in behaviour is still not clear. A possible reason is that in figure 1, the structure of the C_{60} film becomes highly perfect and the anomalous jump near 278 K is reduced due to annealing. This leads to the result that the anomalous jumps in the ranges 263–268 K and 280–283 K can no longer be clearly distinguished, and finally results in the compression of the conductance jump and the widening of the temperature spread of the jump in figure 1(b).

4.3. Effects of gas contamination

Figures 1(c)–4(c) indicate that absorption of air induces the conductivity of the samples to drop by about four orders of magnitude. The difference between the activation energies below and above the jump temperature ranges in figure 1(c) changed less than those in figures 2(c)–4(c). In figures 2(c)–4(c), the activation energies below and above the conductance jump ranges are a few meV and $\sim$1 eV, respectively.

The intercalation of oxygen significantly affects the electrical properties of C_{60} films [20–22]. Unlike alkali metal intercalates, which can transfer a large amount of charge (one electron per alkali metal atom) to C_{60} balls, a very low charge transfer occurs for the case of oxygen intercalation [20–22].

In particular, oxygen decreases the intrinsic conductivity of fullerites by as much as four orders of magnitude [22]. When the sample is exposed to air, O_2 is absorbed into the interface of the films and some of the O_2 diffuses into the lattice of the C_{60} crystal and bonds to the C_{60}, forming some impurity states and reducing the symmetry of the C_{60} ball. So C_{60} in different positions in the film faces bonds differently to the absorbed O_2, which induces the different impurity band energies. Different environments of C_{60} lead to different densities of impurity states. The absorbed O_2 may act as a compensating centre and capture the carriers as well as reducing the conductance of the films. The incorporated O_2 will form deep impurity states, increasing the activation energy of the films.

The adsorbed oxygen plays a remarkable role in the conductivity and activation energy processes [22, 23]. The lower conductivity for C_{60} films also tends to lead to high activation energy, and vice versa. This can be explained by observing that, when introduced interstitially into a fullerene material, molecular oxygen quenches the conductivity and creates deep electronic traps. The more oxygen present in the C_{60} matrix, the deeper these traps are, and thus the higher the activation energy is.

Below 300 K, the activation energies of the samples are very small: some of them are of a few meV; such small values of the activation energy are probably caused by the combination of Sb and absorbed O_2 in crystalline C_{60}. Sb and absorbed O_2 form different electronic states at the band gap of crystalline C_{60}, and also some states have subband gaps that cause some tunnelling of carriers. Alternatively, as the sample has been exposed to the air, most of the Sb is very probably oxygenated, so the surviving Sb is present in very limited amounts, which will result in a low conductivity with a small activation energy. The oxygenation process can be signalled by the lack of recovery of the conductivity after annealing treatments. Above 300 K, large activation energies may be contributed by activation effects of O_2 bonded with

C_{60}. Upon annealing, the absorbed O_2 will be pulled out of the C_{60} solid. The activation energy of the expulsion adds to the activation energy of oxygenated C_{60}, yielding a relatively high (relative to the optical absorption edge) value of $E_a = 2.2$ eV.

Annealing increases the conductivity of the film (shown in region 3 in figure 4(c)) probably both by improving the crystallinity of the films and by driving oxygen out of the interstitial regions. The driving out of oxygen can also be inferred from the relatively small activation in the temperature-drop process shown in figure 4(c).

5. Conclusions

Interesting structure and conductivity properties of C_{60}/Sb bilayers have been studied. Sb doped into C_{60} crystal has some remarkable effects on the C_{60} fcc–sc phase transition. For Sb-doped C_{60} crystal, the fcc–sc transition temperature is higher than that of pristine C_{60} crystal. The smaller grain size of C_{60}/Sb corresponds to an Sb-doped C_{60}-dominated phase transition, indicating that an interfacial phase of Sb-doped C_{60} has formed. The heat treatment destroys the interfacial structure of Sb-doped C_{60}. The absorbed O_2 can also destroy the structure of Sb-doped C_{60} entirely, to the extent that it cannot be recovered after the O_2 desorption. Although our conclusions from the above results are qualitative, to get firm evidence for the intrinsic interaction of Sb and C_{60}, more chemical probing and *in situ* STM study are needed, and such research is being undertaken.

Acknowledgments

One of authors, Dr Xiang Li, thanks Professor J R Sun for instructive discussions. This programme of work was supported by the NSF of China and J G Hou acknowledges the support of the 'QiuShi' Foundation.

References

[1] Pevzner B, Hebard A F and Dresselhaus M S 1997 *Phys. Rev.* B **55** 16 439
[2] Pitsi G, Caerels J and Thoen J 1997 *Phys. Rev.* B **55** 915
[3] Yildirim T, Fisher J E, Harris A B, Stephens P W, Liu D, Brard L, Strongin R M and Smith A B III *Phys. Rev. Lett.* **71** 13 839
[4] Tanigaki K, Hirosawa I, Manako T, Tsai J S, Mizuki J and Ebbesen T W 1994 *Phys. Rev.* B **49** 12 307
[5] Maxwell A J, Brühwiler A P, Arvanitis D and Hasselström J 1998 *Phys. Rev.* B **57** 7312
[6] Yoshinari Y, Alloul H, Brouet V, Kriza G, Holczer K and Forro L 1996 *Phys. Rev.* B **54** 6155
[7] Su J S and Chen Y F 1999 *Appl. Phys. Lett.* **75** 1607
[8] Heiney A P, Fisher J E, McGhie A R, Romanov W J, McCauley J P Jr and Smith A B III 1991 *Phys. Rev. Lett.* **66** 2911
[9] Alers G B, Golding B, Kortan A R, Haddon R C and Theil F A 1992 *Science* **257** 511
[10] Wen C, Li J, Kitazawa K, Aida T, Honma I, Komiyama H and Yamada 1992 *Appl. Phys. Lett.* **61** 2162
[11] Mort J, Ziolo R, Machonkin M, Huffman D R and Ferguson M I 1991 *Chem. Phys. Lett.* **186** 284
[12] Meingast C, Roth G, Pintschovius L, Michel R H, Stoermer C, Kappes M M, Heiney P A, Brard L, Strongin R M and Smith A B III 1996 *Phys. Rev.* B **54** 124
[13] Lommen A N, Heiney P A, Vaughan G B M, Stephens P W, Liu D, Li D, Smith A L, McGhie A R, Strongin R M, Brard L and Smith A B III 1994 *Phys. Rev.* B **49** 12 572
[14] Gadd G E, Kennedy S J, Moricca S, Howard C J, Elcombe M M, Evans P J and James M 1997 *Phys. Rev.* B **55** 14 794
[15] Xu Wentao, Hou J G and Wu Z Q 1998 *Appl. Phys. Lett.* **73** 1367
[16] Hou J G, Xu Wentao, Wang Haiqian and Yang Li 1998 *J. Appl. Phys.* **84** 2906
[17] Xu Wentao and Hou J G 1999 *J. Appl. Phys.* **86** 4660
[18] Xu Wentao and Hou J G 2000 *J. Cryst. Growth* **208** 365

[19] Li Xiang *et al* 2000 *J. Appl. Phys.* **88** 6931
[20] Hamed A, Sun Y Y, Tao Y K, Meng R L and Hor P H 1993 *Phys. Rev.* B **47** 10 873
[21] Han D X, Habuchi H and Nitta S 1998 *Phys. Rev.* B **57** 3773
[22] Arai A, Murakami Y, Suematsu H, Kikuchi K, Achiba Y and Ikemoto I 1992 *Solid State Commun.* **84** 827
[23] Fujimori S, Hoshimono K, Fujita S and Fujita S 1992 *Solid State Commun.* **89** 437